

12-2014

Detection of gravitational wave signals from NS-NS inspirals in presence of non-stationary noise

Wenhui Wang
The University of Texas Rio Grande Valley

Follow this and additional works at: https://scholarworks.utrgv.edu/leg_etd



Part of the [Cosmology, Relativity, and Gravity Commons](#)

Recommended Citation

Wang, Wenhui, "Detection of gravitational wave signals from NS-NS inspirals in presence of non-stationary noise" (2014). *UTB/UTPA Electronic Theses and Dissertations*. 45.
https://scholarworks.utrgv.edu/leg_etd/45

This Thesis is brought to you for free and open access by the Legacy Institution Collections at ScholarWorks @ UTRGV. It has been accepted for inclusion in UTB/UTPA Electronic Theses and Dissertations by an authorized administrator of ScholarWorks @ UTRGV. For more information, please contact justin.white@utrgv.edu, william.flores01@utrgv.edu.

DETECTION OF GRAVITATIONAL WAVE SIGNALS FROM NS-NS
INSPIRALS IN PRESENCE OF NON-STATIONARY NOISE

By

Wenhui Wang


A Thesis Presented to the Graduate Faculty of the College of Science, Mathematics
and Technology in Partial Fulfillment of the Requirements for the Degree of

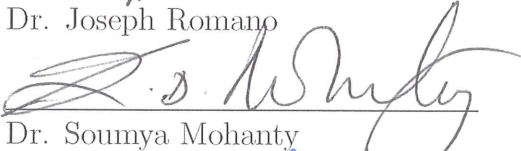
Master of Science

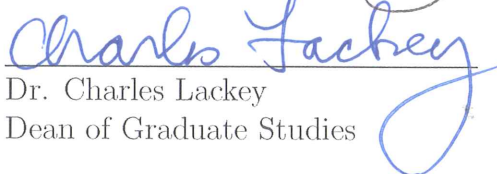
in the field of Physics

Approved by:


Dr. Soma Mukherjee
Thesis Advisor


Dr. Joseph Romano


Dr. Soumya Mohanty


Dr. Charles Lackey
Dean of Graduate Studies

Graduate School

University of Texas at Brownsville

December 2014

Detection Of Gravitational Wave Signals From NS-NS Inspirals In
Presence Of Non-Stationary Noise

A Thesis Presented to the
Faculty of the
College of Science, Mathematics and Technology
The University of Texas at Brownsville

in Partial Fulfillment
of the Requirements for the Degree
Master of Science

by

Wenhui Wang

December 2014

© Copyright

by

Wenhui Wang

December 2014

All Rights Reserved.

University of Texas at Brownsville

Date: December 2014

Author: Wenhui Wang

Title: Detection Of Gravitational Wave Signals From
NS-NS Inspirals In Presence Of Non-Stationary Noise

Department: Physics

Degree: M.S. Convocation: December Year: 2014

Permission is herewith granted to University of Texas at Brownsville to circulate and to have copied for non-commercial purposes, at its discretion, the above title upon the request of individuals or institutions.

Wenhui Wang

Signature of Author

THE AUTHOR RESERVES OTHER PUBLICATION RIGHTS, AND NEITHER THE THESIS NOR EXTENSIVE EXTRACTS FROM IT MAY BE PRINTED OR OTHERWISE REPRODUCED WITHOUT THE AUTHOR'S WRITTEN PERMISSION.

THE AUTHOR ATTESTS THAT PERMISSION HAS BEEN OBTAINED FOR THE USE OF ANY COPYRIGHTED MATERIAL APPEARING IN THIS THESIS (OTHER THAN BRIEF EXCERPTS REQUIRING ONLY PROPER ACKNOWLEDGEMENT IN SCHOLARLY WRITING) AND THAT ALL SUCH USE IS CLEARLY ACKNOWLEDGED.

ACKNOWLEDGMENTS

I would like to thank my advisor Dr. Soma Mukherjee for all the support she has provided to me during the entire length of my graduate education from every aspect and leading me to the field of gravitational waves. She is a mentor and also a friend. I thank Dr. Soumya D. Mohanty and Dr. Joseph Romano for being committee members and for the comments on my thesis. I would also like to thank all of the professors for classes to show me the way to the study of gravitational waves and friends for help all the time. My deep thanks for my family for supporting me all the time. Finally I express my heartfelt gratitude to the Center for Gravitational Wave Astronomy for the financial assistance throughout my graduate education. This research is supported by National Science Foundation grant # NSF 1205585 (2012) (J. D. Romano, S. Mukherjee and S. D. Mohanty).

ABSTRACT

Wang, Wenhui , “**Detection Of Gravitational Wave Signals From NS-NS Inspirals In Presence Of Non-Stationary Noise**”, Master of Science Thesis, University of Texas at Brownsville, Brownsville, TX, 2014

Gravitational Wave (GW) detection is an important and inspiring project. Once detected, it will open a new window to understand the universe. The laser interferometer GW detectors, specially LIGO, is the most sensitive detectors at the moment, which can detect GW signal as weak as 10^{-21} . Chirp signal generated by neutron star binaries is a well modeled waveform. One goal of LIGO is to study chirp signal detection. In this field, matched filtering is a widely used method. But since LIGO noise is non-stationary, which will weaken the efficiency of general matched filtering. In this work, a modified matched filtering is built to take non-stationary into account.

TABLE OF CONTENTS

| | | |
|----------|--|-----------|
| 1 | Introduction | 1 |
| 1.1 | Introduction to the Gravitational Waves | 1 |
| 1.2 | History of Detection | 4 |
| 1.3 | Interferometers | 5 |
| 1.4 | Gravitational Wave Sources | 7 |
| 2 | LIGO data | 8 |
| 2.1 | How Data is Archived | 8 |
| 2.2 | LSC | 8 |
| 2.3 | LIGO Noise | 10 |
| 2.4 | Sensitivity | 10 |
| 3 | Review of Matched Filtering Method and Application | 12 |
| 4 | Simulation and Results | 15 |
| 4.1 | Simulation of Non-stationary Noise | 16 |
| 4.2 | Chirp Signal | 17 |
| 4.3 | Constructing Data and the Output of Matched Filtering Method | 20 |
| 5 | Conclusion | 32 |
| A | Chirp Signal | 39 |
| B | Output of Matched Filter for LIGO and GaussianSine Data | 40 |

LIST OF FIGURES

| | | |
|----|---|----|
| 1 | GWs effect on a ring of particles | 3 |
| 2 | Prof. Weber working on his antenna Source | 5 |
| 3 | Diagram of LIGO | 6 |
| 4 | LIGO Hanford (LHO) Aerial 1 | 6 |
| 5 | The process of data acquisition, data processing and template based analysis. | 9 |
| 6 | Interferometer noise in science runs $S1 - S5$ | 11 |
| 7 | The typical sensitivity of detectors during the S6 run | 11 |
| 8 | Principle of matched filter | 14 |
| 9 | Variance of LIGO data from LHO S6 run ‘H1: LSC-DARM_ERR’. | 15 |
| 10 | Non-stationary noise standard deviation vector generated by sine func- tion with 4 peaks. | 16 |
| 11 | Non-stationary noise standard deviation vector generated by sine func- tion with 8 peaks | 17 |
| 12 | Chirp signal generated by BNS system | 19 |
| 13 | White noise and injected chirp signal | 20 |
| 14 | Chirp signal and built non-stationary noise sets | 23 |
| 15 | Output SNR of MF/MMF for 4 segments standard deviation | 24 |
| 16 | Output SNR of MF/MMF for 8 segments standard deviation | 25 |

| | | |
|----|--|----|
| 17 | Output SNR of MF/MMF for 4 segments standard deviation where signal injected from 10th second | 26 |
| 18 | LIGO noise and chirp signal 1 | 28 |
| 19 | Output SNR of MF/MMF for LIGO noise 1 | 29 |
| 20 | LIGO noise and chirp signal 2 | 30 |
| 21 | Output SNR of MF/MMF for LIGO noise 2 | 31 |

CHAPTER 1

INTRODUCTION

1.1 INTRODUCTION TO THE GRAVITATIONAL WAVES

In 1916, Albert Einstein published the General Theory of Relativity (GR), which predicted the existence of Gravitational Waves (GWs) [1, 2, 3]. Based on GR, the whole universe is a curved space described by a 4-dimensional space-time, which is produced by mass. John Wheeler succinctly summarized GR puts as “Spacetime tells matter how to move; matter tells spacetime how to curve.” Mass in (non-spherical, nonuniform) motion is the source of perturbations or ripples of curved spacetime. GWs are the propagating ripples, produced by accelerating mass and emitted as gravitational radiation, traveling at the speed of light [4]. By solving Einstein’s equation, we can get the gravitational waveforms for different sources. But since there is no such thing yet as a general solution [4], we only consider the simplest linearized vacuum Einstein Equation, where the metric is written

$$g_{\alpha\beta}(x) = \eta_{\alpha\beta} + h_{\alpha\beta}(x) \tag{1}$$

where $\eta_{\alpha\beta} = \text{diag}(-1, 1, 1, 1)$, and $h_{\alpha\beta}(x)$ are small quantities called *metric perturbations* [5, 4, 6].

Substituting this into the Einstein Equation, it turns out that $h_{\alpha\beta}(x)$

satisfies the wave equation,

$$\left(-\frac{\partial^2}{\partial t^2} + c^2 \vec{\nabla}^2\right)h_{\alpha\beta} = 0 \quad (2)$$

under *Lorentz gauge conditions*. For this kind of wave function, the solutions can be expressed as

$$h_{\alpha\beta}(x) = a_{\alpha\beta}(x)e^{ik_\mu x^\mu} \quad (3)$$

where $a_{\alpha\beta}(x)$ is a symmetric 4×4 matrix of constant amplitudes, $k_\mu = (-\omega, \vec{k})$ and $x^\mu = (t, \vec{x})$.

There are only two independent components of $h_{\alpha\beta}$, the two polarization h_+ and h_\times . (For details, please see [4, 6]). When GWs pass perpendicularly to a plane, they will change the distance of two particles in the plane. One direction is stretched while the perpendicular direction will be shortened. It can be shown by the effect of GWs on a ring of particles as illustrated in Fig. 1. The change in distance between particles is δl , and $\frac{\delta l}{l}$ is proportional to $h_{\alpha\beta}$. For astronomical objects, the amplitude of the wave strain arriving on Earth is of order or less than 10^{-21} [7] and the maximum change of distance the ground-based interferometer can measure is 10^{-18} m. Thus, it requires the ground-based interferometers to be kilometer scales to detect the GWs of the distant astronomical sources.

From the above analysis, we see that GW signals are usually very weak. For a typical solar mass binary system, the amplitude when it reaches to earth is 10^{-20} , so the strong and violent cosmic events caused by massive objects provide good

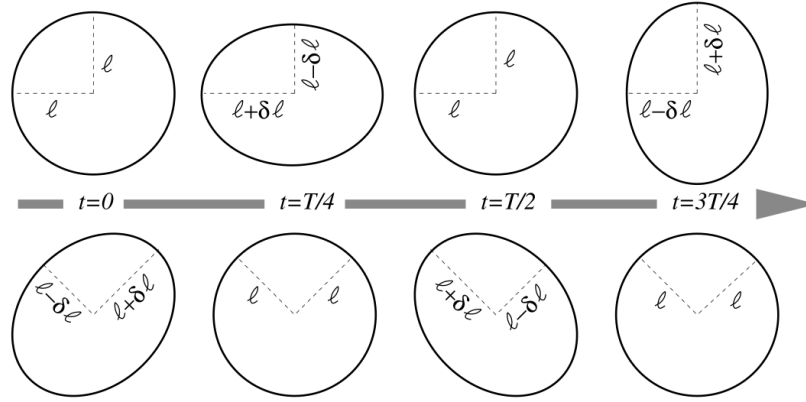


Figure 1: GWs effect on a ring of particles [5]

experiments.

Why is the detection of GWs so important? As far as we know, every time a new band of Electromagnetic(EM) wave is available to detect, our understanding is always expanded and a lot of new discoveries are made. But GW is not only a new band, it is a totally new window to explore the universe. So we can expect what a great promotion it will be for all the principles after it is detected. Compared to EM waves, GWs are produced by the curved spacetime itself so it can reveal a lot of properties of the curvature caused by the objects, which provide a direct way to study objects like Black Holes, which is dark in EM bands. Besides, GWs propagate in the spacetime with no distortion and no absorption. It can bring the original information about the events. Another important thing is that GWs are predicted by Einstein's GR theory, so this is a direct way to check if GR works as predicted [5, 8, 6].

Although not detected directly, there are some indirect evidences showing the existence of GWs. In 1993, Joseph Taylor and Russell Hulse were awarded Nobel

Prize for their work to measure accurately the influence of gravitational waves on a binary pulsar $PSR1913 + 16$, which is in good agreement with predictions [9, 10]. And in March 2014, the scientists from Harvard-Smith-Center announced they have found the B-mode of Cosmic Microwave Background, which is the first direct image of GWs [11].

1.2 HISTORY OF DETECTION

Since GWs can lead to a new epoch of our understanding, scientists have been trying to detect them for about fifty years. The first detector, Weber's bar, is a cylinder of aluminum built by Joseph Weber (see Fig. 2). When there is gravitational wave, the length of the cylinder will change, which will transfer to a voltage to be read. But since Weber's bar can only detect signals on order of 10^{-16} , much higher than the GWs signal expected at earth, although Weber claimed several detections, no real detection was made at that time. But a global network of new enhanced Weber's bars are much more promising.

After Weber's bar [12], his student Robert Forward constructed the first laser interferometer detector. But since GWs are so weak, typically $\delta l \sim 10^{-18}$ m, so to achieve the sensitivity of the signal requires the arms of the detector to be kilometers long based on $\delta l/l \sim 10^{-21}$, which requires collaborations. And to claim the detection of a signal, one needs coincidence of the same detection from different detectors. Therefore, a network of detectors is important and necessary. At the moment, there are six interferometer detectors in the world. The Laser Interferometer of Gravitational Wave Observatory (LIGO) in US has three interferometers [13, 14, 15]. Two

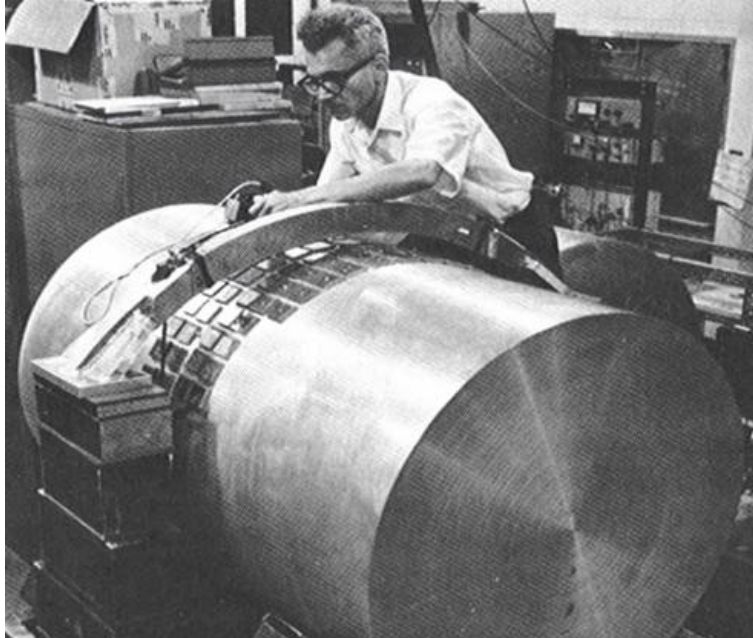


Figure 2: Prof. Weber working on his antenna Source: <http://www.physics.umd.edu/GRE/GWdetect.htm>

are in Hanford, one with $4km$ arms and the other one with $2km$ arms. The third one is in Livingston, with $4km$ arms. Besides, there are VIRGO [16]. with $3km$ arms, British-German collaboration GEO 600 [17, 18] having $600m$ arms and TAMA [19] with $300m$ arms. Among all these detectors, the most sensitive detector is LIGO, based on which we conduct our research.

1.3 INTERFEROMETERS

LIGO is a much more complicated, modified and advanced Michelson interferometer [13, 14, 15]. The laser is split into two equal light beams by the beam splitter and reflected by the two mirrors at the end of the two arms. So we can get the interference phase of the two light beams. If there comes a gravitational wave, it will change the distances between the mirrors and the light sensing diode. To be

more detailed, as we discussed above, one arm will be stretched while the other arm will be squeezed. Thus, we can get different interference phase to claim a signal.

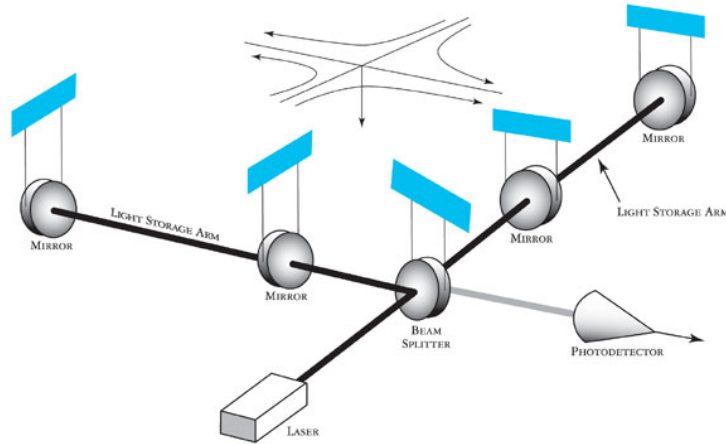


Figure 3: Diagram of LIGO

Fig. 4 shows the $4km$ interferometer in Hanford.



Figure 4: LIGO Hanford (LHO) Aerial 1

1.4 GRAVITATIONAL WAVE SOURCES

There are four main types sources of GWs. 1) Coalescing Compact Binary Systems, such as Neutron Star(NS)-NS, Black Hole(BH)-NS, BH-BH. These events emit strong and well-modeled GWs and are the central systems we focus on in this paper. 2) Asymmetric Core Collapse Supernovae, which emits weak and unmodeled bursts. 3) Spinning neutron stars, whose radiation waveform is monotonic but has long duration. 4) Cosmic GWs stochastic background comes from the residue of the Big Bang, with long duration [20, 21].

CHAPTER 2

LIGO DATA

2.1 HOW DATA IS ARCHIVED

Fig. 5 shows the process of data acquisition, data processing and template based analysis [22]. The LIGO data is a collection of several thousand channels sampled at a rate of 16384Hz. Upon acquisition, the raw data stream will be reduced through three stages to extract the useful part of data. There are four data sets, from Level 0 to Level 3. The raw data is Level 0, also named “Full IFO Data Stream”, which is archived in FRAME format. In stage 1, only 10% of Level 0 data is kept to Level 1 for detector diagnostic study. In stage 2, the data is further reduced to about 1% for more detailed science analysis. Level 2 data will contain basic IFO strain data and data quality channels. The level 3 data is the “Whitened GW Strain Data”. It contains the best estimated whitened GW strain, which is free from instrumental artifacts as much as possible. It will include all the relevant whitening coefficients, regression and calibration information from Level 2 data [23]. LIGO data is available from the DATA GRID on LIGO website (<https://www.lsc-group.phys.uwm.edu/lscdatagrid/resources/data/index.html>).

2.2 LSC

As mentioned above, there has been no direct detection of GWs yet. Thus it is inspiring to make a detection. The LIGO Scientific Collaboration (LSC) is a group of scientists seeking to make the first direct detection of GWs, and to use

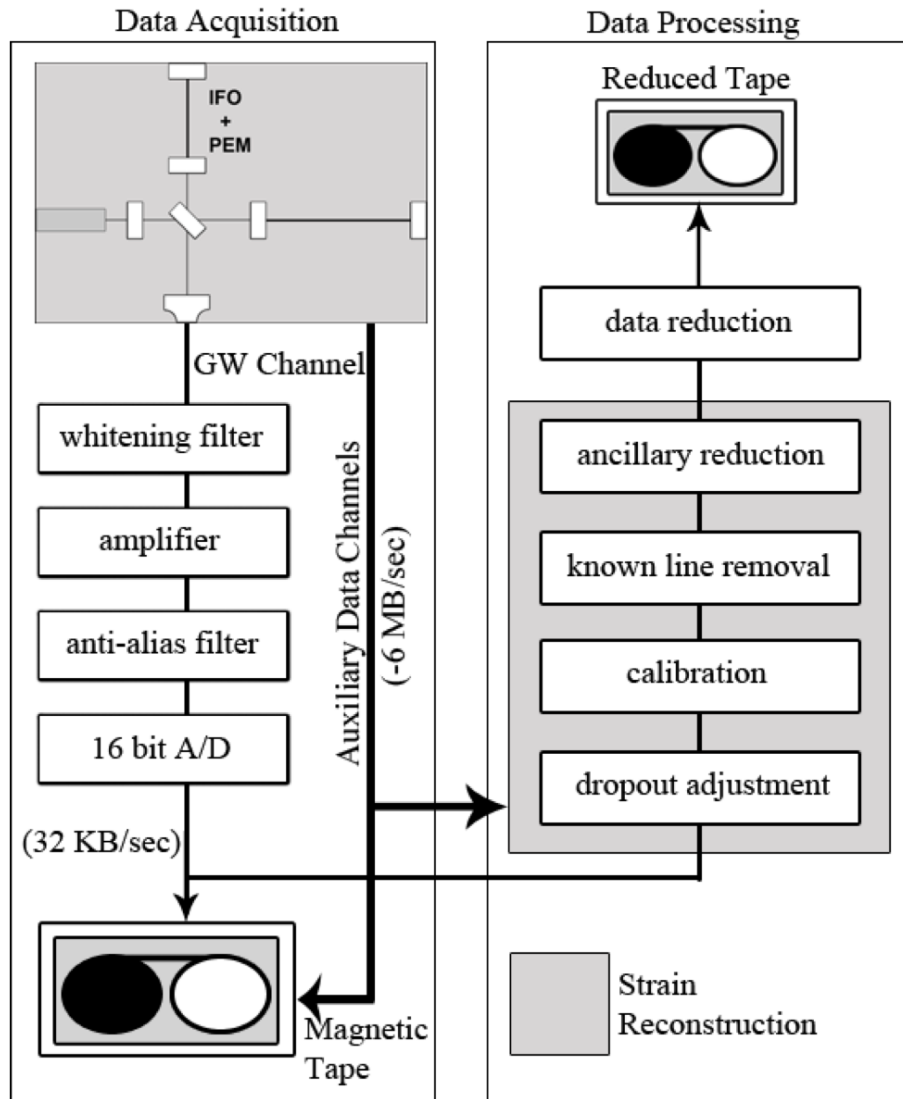


Figure 5: The process of data acquisition, data processing and template based analysis.

them to extend the field of astronomy. The LSC conducts research on and develops technologies for gravitational-wave detection and also detectors. Founded in 1997, the LSC now contains more than 900 scientists and 16 countries worldwide. It carries out the science of LIGO observatories and the GEO600 detector. For more detailed information about LSC, please see <http://www.ligo.org/about.php>.

2.3 LIGO NOISE

Since GWs are so weak compared to the noises, a very important research problem is how to remove the noises from the data. There are basically two classes of noise: displacement noise and sensing noise [24]. Displacement noises cause motions of the test masses or their mirrored surfaces. Sensing noises will limit the ability to measure those motions, even without the test mass motion. The lowest frequency noise of displacement noises is seismic noise. The seismic noise, transmitted to the mirrors by housing and pendulums, dominates below 45Hz, a little bit larger than designed. There is also the mechanical thermal noise, which causes arm length changes through thermal excitation of the test mass pendulums (suspension thermal noise) [25] and thermal acoustic waves that perturb the test mass mirror surface (test mass thermal noise) [26]. Above about 200Hz, the dominant contribution is the photon shot noise, combined with counting statistics of photons at the photodiode [13, 5]. The above three noises are described in Fig. 6.

2.4 SENSITIVITY

The initial designed sensitivity of LIGO detectors were in the frequency band 40 – 7000Hz, and capable of detecting a GW strain amplitude to 10^{-21} [13]. The typical sensitivity of the detectors during the S6 run is shown in Fig. 7.

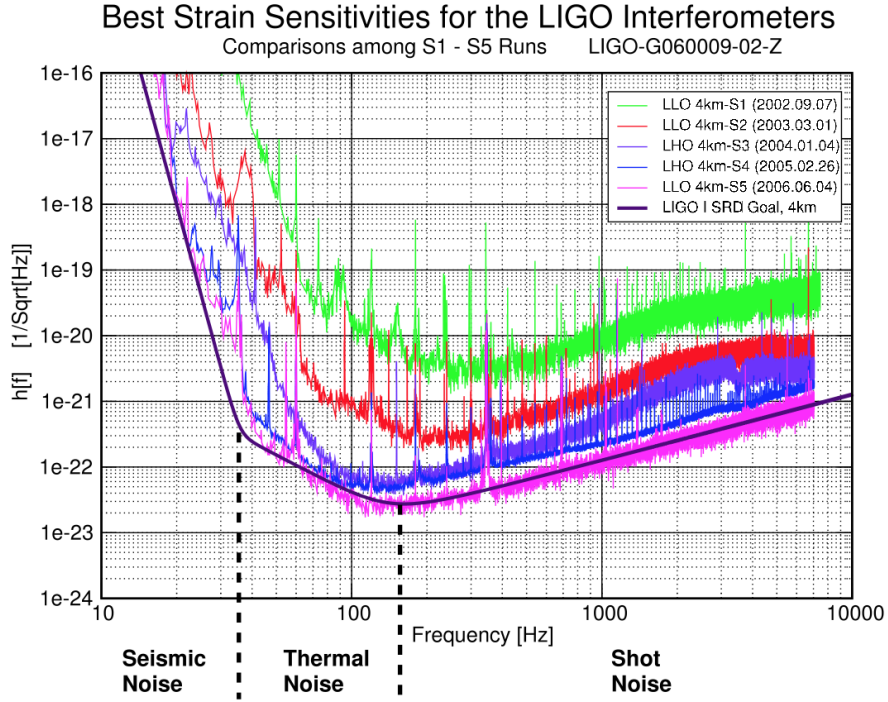


Figure 6: Interferometer noise in science runs $S1 - S5$. The black curve is the design goal of LIGO [5].

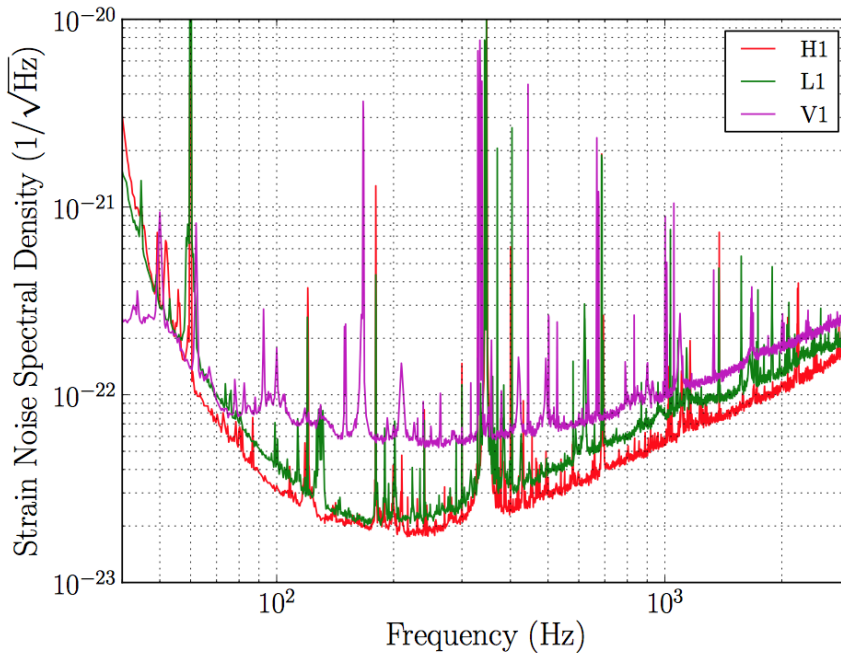


Figure 7: The typical sensitivity of detectors during the S6 run [27].

CHAPTER 3

REVIEW OF MATCHED FILTERING METHOD AND

APPLICATION

Matched filter is a filter whose impulse response is matched to the signal. It is widely used in signal detection and the detection is to distinguish between the hypotheses [5, 28, 29]

$$\mathcal{H}_0 : x[n] = w[n] \quad n = 0, 1, \dots, N - 1 \quad (1)$$

$$\mathcal{H}_1 : x[n] = s[n] + w[n] \quad n = 0, 1, \dots, N - 1 \quad (2)$$

where $s[n]$ is signal and $w[n]$ is white gaussian noise with σ^2 .

The probabilities under this hypotheses is

$$p(\mathbf{x}; \mathcal{H}_0) = \frac{1}{(\sqrt{2\pi})^N |\mathbf{C}|^{1/2}} e^{-\frac{1}{2} \langle \mathbf{x}, \mathbf{x} \rangle} \quad (3)$$

$$p(\mathbf{x}; \mathcal{H}_1) = \frac{1}{(\sqrt{2\pi})^N |\mathbf{C}|^{1/2}} e^{-\frac{1}{2} \langle \mathbf{x} - \mathbf{s}, \mathbf{x} - \mathbf{s} \rangle} \quad (4)$$

Following the Neyman-Pearson (NP) theory, the detector decides \mathcal{H}_1 if the likelihood exceeds or the detection statistic of general Matched Filtering when the noise is white and stationary exceeds a threshold, in Eq. 5 .

$$T(x) = \sum_{n=0}^{N-1} x[n]s[n] = \langle \mathbf{x}, \mathbf{s} \rangle > \gamma' \quad (5)$$

where $x[n]$ is the data time series and $s[n]$ is the signal series. The output is also known as inner product of data series \mathbf{x} and signal vector \mathbf{s} , written as $\langle \mathbf{x}, \mathbf{s} \rangle$. The detector of Eq. 5 is referred to as a replica-correlator, as shown in Fig. 8 (a).

The detection statistic can also be interpreted in this way. If $x[n]$ is the input to a finite impulse response filter whose impulse is $h[n]$, where $h[n]$ is defined as

$$h[n] = \begin{cases} s[N - 1 - n] & n = 0, 1, \dots, N - 1 \\ 0 & \textit{otherwise} \end{cases} \quad (6)$$

then the output of the filter at time n is

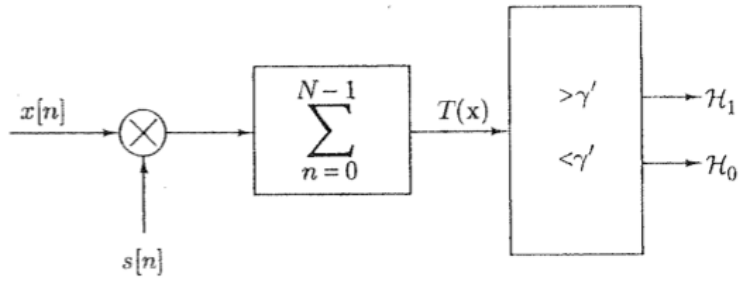
$$y[n] = \sum_{k=0}^n h[n - k]x[k], \quad \textit{for } n \geq 0 \quad (7)$$

so, replacing $h[n - k]$ by $s[k]$, the output of the filter becomes

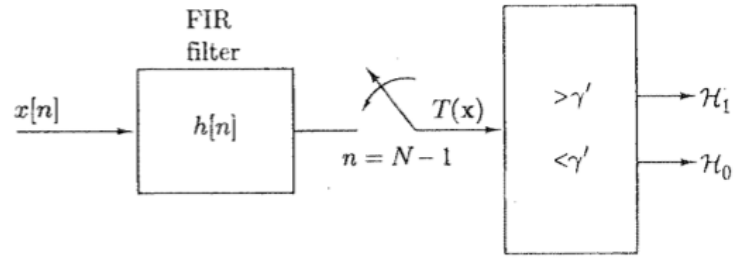
$$y[N - 1] = \sum_{k=0}^{N-1} s[k]x[k] \quad (8)$$

which is the inner product of signal and data as detection statistic requires. This is called a matched filter. The detector is shown in Fig. 8 (b).

The matched filter gives the maximum signal-to-noise ratio (SNR) among all possible linear filters in the ideal case of Gaussian-distributed noise, assuming that the template corresponds exactly to the signal potentially in the data [30, 31].



(a)



$$h[n] = \begin{cases} s[N-1-n] & n = 0, 1, \dots, N-1 \\ 0 & \text{otherwise} \end{cases}$$

(b)

Figure 8: (a) is the replica-correlator and (b) is the Matched filter [28]

CHAPTER 4

SIMULATION AND RESULTS

The previous three chapters show that matched filtering is an optimal method to detect signals when the noise is white and gaussian, and it is widely used in GW detection for LIGO. But when the noise is non-stationary, its efficiency is reduced. So for LIGO data, in which the noise is non-stationary as shown in Fig. 9, a modified matched filtering method that includes time-varying noise is needed for better detection.

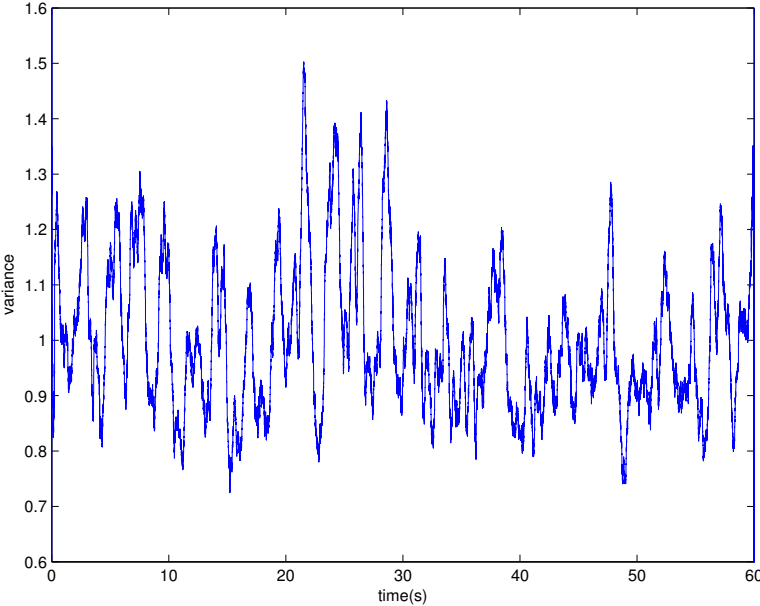


Figure 9: Variance of LIGO data from LHO S6 run ‘H1: LSC-DARM_ERR’. The horizontal axis is time and the vertical axis is variance. Sampling frequency is 2048 Hz.

4.1 SIMULATION OF NON-STATIONARY NOISE

We observe that LIGO noise variance changes on a scale of few seconds. To construct a data set with slowly varying noise, that is similar to variations seen in LIGO noise, we built two standard deviation(variance) models with sinusoidal variation, and each model has different amounts of peaks. The first model(Fig. 10) shows a varying standard deviation(variance) set on a time scale of about 10seconds. The second model(Fig. 11) has a relativistic faster and stationary variation.

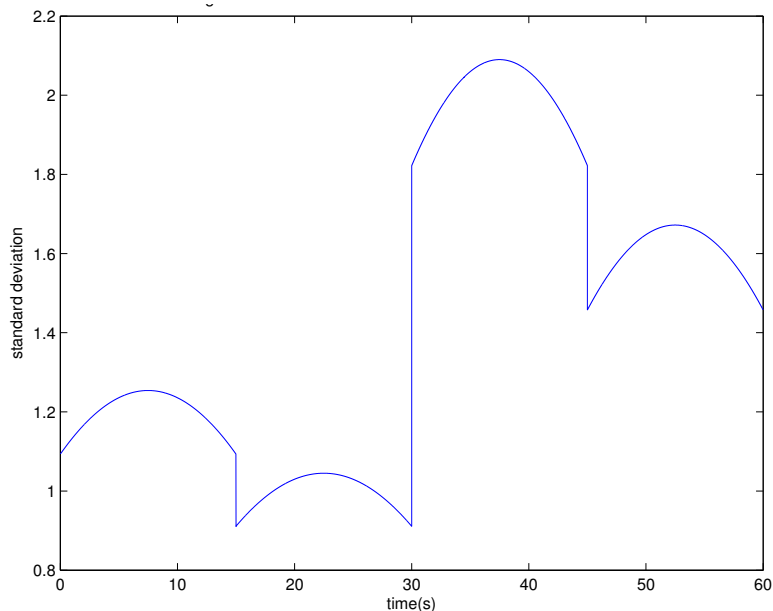


Figure 10: Non-stationary noise standard deviation vector generated by sine function with 4 peaks and is composed of 4 segments with different values. The the horizontal axis is time and the vertical axis is the magnitude of standard deviation vector we are going to apply to white noise.

As shown in the above two figures, the standard deviation changes slowly among every segments but between different segments, it fluctuates. In the following sections, we will make a comparative analysis of how a general matched filter(GMF) responds to the non-stationary noise and how a modified matched fil-

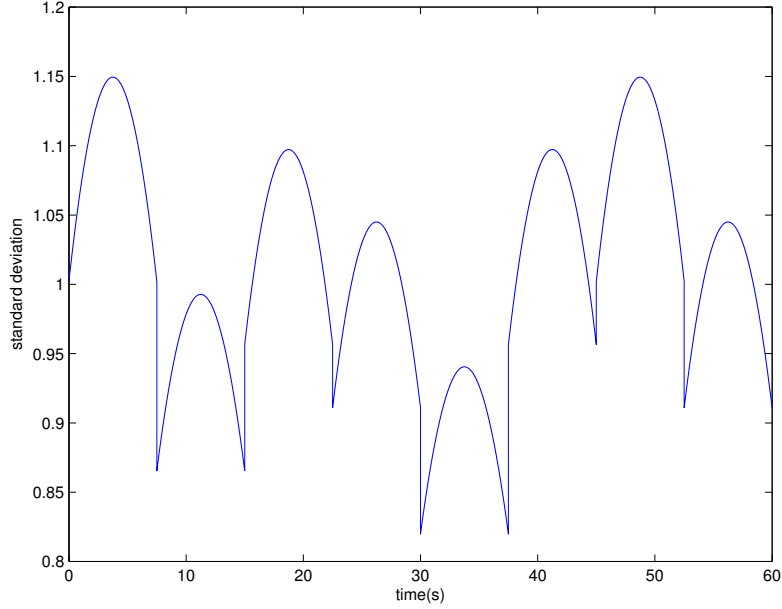


Figure 11: Non-stationary noise standard deviation vector generated by sine function with 8 peaks. This standard deviation vector is combined with 8 segments. This one is much more stationary compared to the above 4 peaks standard deviation vector.

ter(MMF) responds.

4.2 CHIRP SIGNAL

After preparing the non-stationary noise, we calculated the chirp signal with certain parameters and waveforms. The response of an interferometric detector to a GW signal emitted by an inspiral of a compact BNS system can be written as:

$$h(t; \mathcal{A}, t_a, \xi, \Phi) = \mathcal{A}a(t - t_a, \xi) \cos[\phi(t - t_a, \xi) + \Phi] \quad (1)$$

here, \mathcal{A} is related to the distance to the binaries, the orientation of the orbital plane of the binary and the orientation of the detector [32]. Also, t_a is the arrival time of the chirp signal, ξ is the chirp time and ϕ is the phase of waveform. The expression

for \mathcal{A} is

$$\mathcal{A} = 1.92 \times 10^{-23} \left[\frac{\xi}{25.0} \right]^{-1} \left[\frac{r}{100 Mpc} \right]^{-1} \left[\frac{f}{40 Hz} \right]^{-2} \quad (2)$$

The other part of the amplitude varying with time is

$$a(t, \xi) = \left[1 - \frac{t}{\xi} \right]^{-1/4} \quad (3)$$

The phase of the waveform at given time t :

$$\phi(t, \xi) = 2\pi \int_0^t f(t', \xi) dt' \quad (4)$$

The instantaneous frequency is given by

$$f(t, \xi) = f_a a(t, \xi)^{3/2} \quad (5)$$

where f_a is the low frequency cutoff.

And chirp time ξ , which governs the rate of the increase of the instantaneous frequency is given by

$$\xi = 34.54 \left[\frac{\mathcal{M}}{M_\odot} \right]^{-5/3} \left[\frac{f_a}{40 Hz} \right]^{-8/3} \text{ sec} \quad (6)$$

The chirp mass is

$$\mathcal{M} = (\mu^3 M^2)^{1/5} \quad (7)$$

The lower cutoff of the instantaneous frequency f_a , dominated by t_a , is to avoid

seismic noise. Usually, it is set to 40Hz. And the higher cutoff f_c is set to 1000Hz according to the detector's sensitive frequency range as shown in Fig. 7.

In this work, we assume the masses of the binaries are both $1.4M_\odot$. The chirp time for this BNS system is $\xi = 24.8381$ seconds. The result is shown in Fig. 12. (For the simulation, please see Appendix A).

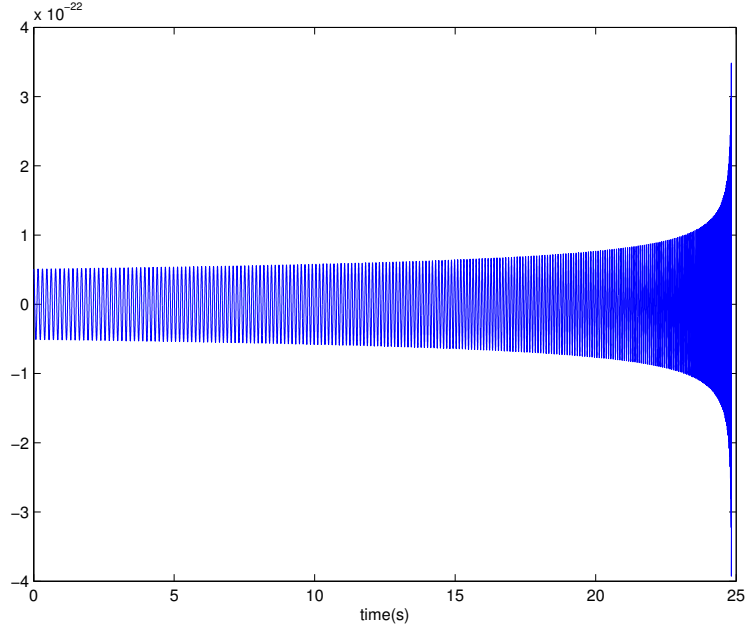


Figure 12: Chirp signal generated by NS-NS system. ($m_1 = m_2 = 1.4M_\odot$, $\xi = 24.8381$ seconds, $r = 38$ Mpc and sampling frequency is 2048Hz). The horizontal axis is time in second and the vertical axis is strain of chirp signal. The signal shown here is original without any normalization.

As mentioned in Sec. 1.1, GW signal is very weak compared to the LIGO noise. In Fig. 13, it is obvious how weak the chirp signal is.

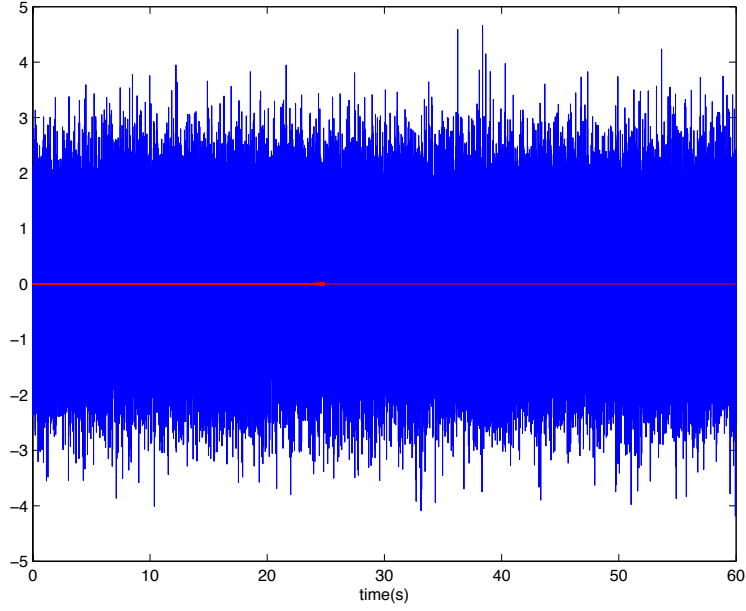


Figure 13: White noise and injected chirp signal. The blue background is white noise and the red small signal is the chirp signal with SNR= 1.

4.3 CONSTRUCTING DATA AND THE OUTPUT OF MATCHED FILTERING METHOD

Following the idea of matched filter, for the chirp signal, we can write signal as the combination of two templates, as shown in Eq. 8

$$\begin{aligned}
 s[n] &= Aa_n \cos(\phi_n + \phi_0) \\
 &= Aa_n (\cos \phi_n \cos \phi_0 - \sin \phi_n \sin \phi_0) \\
 &= \alpha a_n \cos \phi_n - \beta a_n \sin \phi_n \\
 &= \alpha q_{0,n} - \beta q_{\pi/2,n}
 \end{aligned} \tag{8}$$

where $\alpha q_{0,n}$ and $\beta q_{\pi/2,n}$ are templates with SNR=1 and arrival time at 0 second.

The original phase of $\alpha q_{0,n}$ is 0 and $\beta q_{\pi/2,n}$ is $\pi/2$.

Under NP theory, the detection statistic of chirp signal is Eq. 9 when the arrival time and original phase are unknown.

$$\begin{aligned}
T(\mathbf{x}) &= -\frac{1}{2} (\langle \mathbf{x} - \mathbf{s}, \mathbf{x} - \mathbf{s} \rangle - \|\mathbf{x}\|^2) \\
&= \langle \mathbf{x}, \mathbf{s} \rangle - \frac{1}{2} \|\mathbf{x}\|^2 \\
&= \alpha \langle \mathbf{x}, \mathbf{q}_0 \rangle + \beta \langle \mathbf{x}, \mathbf{q}_{\pi/2} \rangle - \frac{1}{2} (\alpha^2 + \beta^2)
\end{aligned} \tag{9}$$

To maximum α and β in Eq. 10,

$$\frac{\partial \Lambda}{\partial \alpha} = \frac{\partial \Lambda}{\partial \beta} = 0 \tag{10}$$

we get Eq. 11

$$\begin{aligned}
\alpha &= \langle \mathbf{x}, \mathbf{q}_0 \rangle = A \cos \phi_0 \\
\beta &= \langle \mathbf{x}, \mathbf{q}_{\pi/2} \rangle = A \sin \phi_0
\end{aligned} \tag{11}$$

Thus, the SNR of signal and phase are maximized with Eq. 12

$$\begin{aligned}
A^2 &= \alpha^2 + \beta^2 \\
\phi &= \arctan \left(\frac{\beta}{\alpha} \right)
\end{aligned} \tag{12}$$

If we put Eq. 11 back to Eq. 9, we can find that

$$\begin{aligned}
T(\mathbf{x}) &= \langle \mathbf{x}, \mathbf{q}_0 \rangle^2 + \langle \mathbf{x}, \mathbf{q}_{\pi/2} \rangle^2 - \frac{1}{2} (\langle \mathbf{x}, \mathbf{q}_0 \rangle^2 + \langle \mathbf{x}, \mathbf{q}_{\pi/2} \rangle^2) \\
&= \frac{1}{2} (\langle \mathbf{x}, \mathbf{q}_0 \rangle^2 + \langle \mathbf{x}, \mathbf{q}_{\pi/2} \rangle^2) \\
&= \frac{1}{2} A^2
\end{aligned} \tag{13}$$

So, we use the output SNR as the detection statistic of matched filter, which is $(\langle \mathbf{x}, \mathbf{q}_0 \rangle^2 + \langle \mathbf{x}, \mathbf{q}_{\pi/2} \rangle^2)$.

With the above non-stationary noise sets generated by sinusoidal wave function, white noise and the waveform template, we constructed our data by injecting the chirp signal into the noise as shown in Fig. 14. Then we passed this data to general matched filter(MF) to see how different non-stationarity will affect the output of matched filter. The results, which are the detection statistic, also known as the outputs of matched filtering, are shown as the blue line in the following figures.

For general matched filtering, the *PSD* or *FFT* of the time series is calculated for the whole time series . Thus, the non-stationarity buried in time-varying time series is omitted. But when use the MMF method, the time series is cut into smaller segments. This method calculates the spectrum of every small time series segment. In this case, the non-stationarity is included by using time series segments with assumption that the noise is quasi-stationary in each segment. [33]. The difference of general matched filtering and modified matched filtering is shown in the following

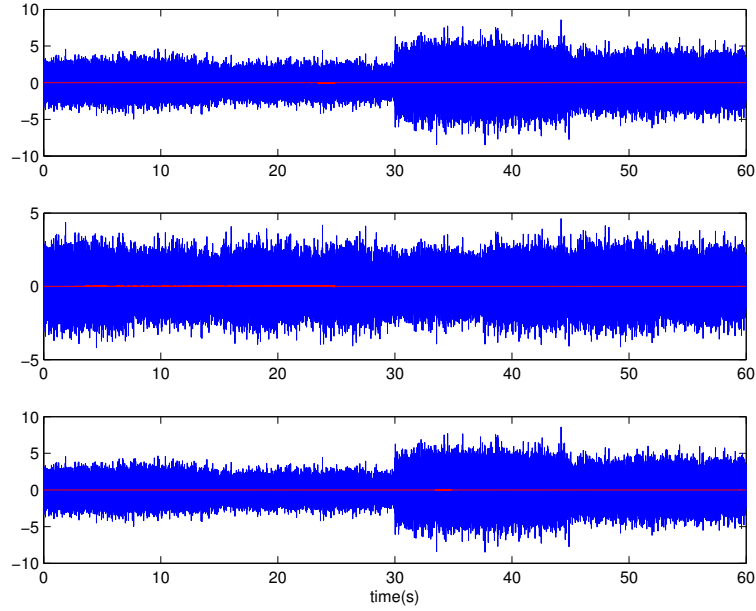


Figure 14: This figure represents the chirp signal injected into different non-stationary sets. The the horizontal axis shows time and the the vertical axis shows amplitude of noise and signal with SNR 1. The above and bottom panel are built by using standard deviation vector in Fig. 10, the difference is the above one the signal is injected from beginning and the bottom one is at 10th second. The middle panel is using Fig. 11 and signal injected at the beginning.

figures.

The result for standard deviation vector set 1, which has 4 segments, is shown in Fig. 15 and for 8 segments shown in Fig. 16. For this two data models, the chirp signal is injected at 0 second. For the non-stationary noise with 8 peaks, which changes slowly between peaks, it will not cause a big effect to inject the signal at any time. But for non-stationary noise built with 4 peaks standard deviation vector, since the variance changes more from peak to peak, the output will be different when signal is injected at different time. Thus, besides injecting chirp signal at the beginning, we also built data model with chirp signal injected at 10th second, which

lies between peak 2 and peak three of standard deviation vector 1. The output is shown in Fig. 17.

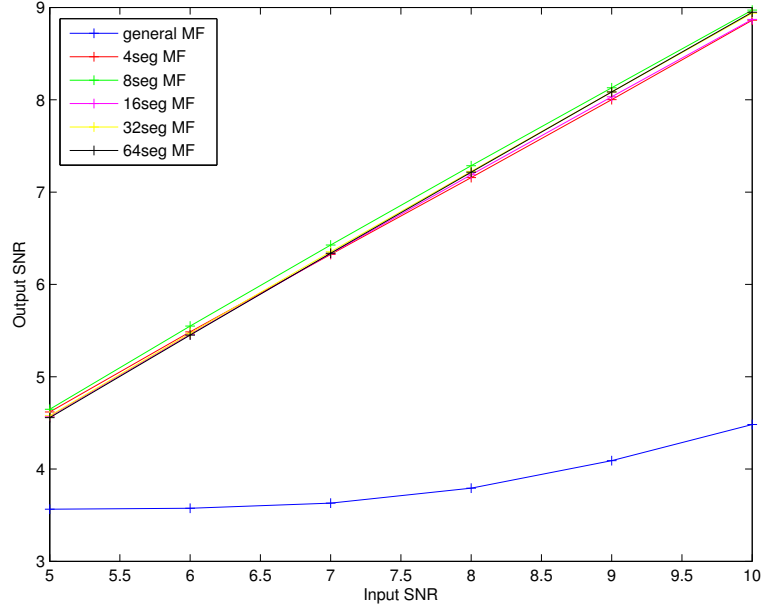


Figure 15: This figure represents the results of detection by the modified matched filter(MMF) with the variance vector divided into 4 segments, when the noise is non-stationary. The the horizontal axis shows the SNR of injected signal and the the vertical axis shows the MF/MMF output SNR. This noise model in this study is shown in Fig. 10 and Fig. 14 above panel. The blue curve represents the output of the search using a standard matched filter(MF). The other curves represent the same when a MMF is used. The different colors show results for different segmentation of the data. It is clear from the figure that the MMF has a significantly better performance than a regular MF. In this study(slow non-stationary), the different segmentations didn't differ from each other in the output.

From these three figures, we can see that if the noise is very close to stationary, then both general matched filter and matched filter with segments will work. But if the noise is non-stationary, as shown in Fig. 10, when the arrival time of signal is different, the output of matched filter will be different. For Fig. 15, the arrival time of chirp signal is 0 *second*, which means the signal residents in the stationary

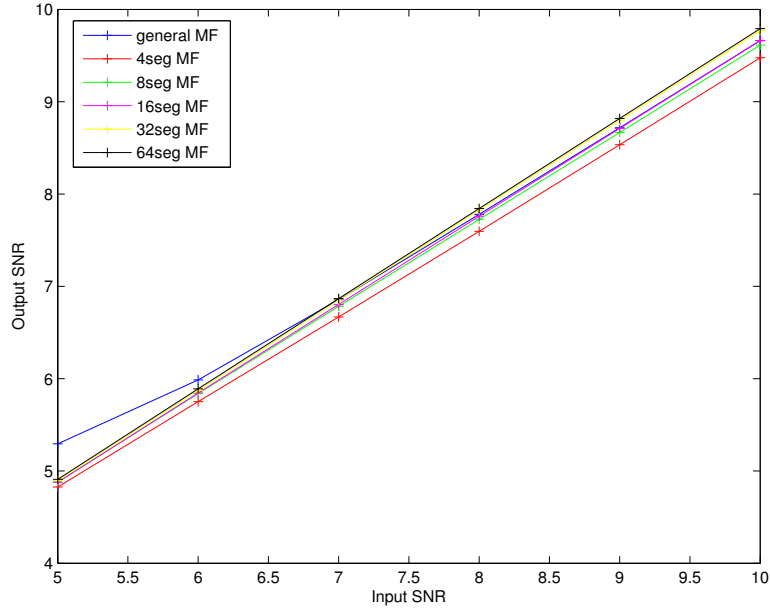


Figure 16: This figure represents the results of detection by the MMF with the variance vector divided into 8 segments. The horizontal axis shows the SNR of injected signal and the vertical axis shows the MF/MMF output SNR. This noise model in this study is shown in Fig. 11 and the chirp signal is injected from the beginning in Fig. 14 middle panel. The blue curve represents the output of the search using a standard matched filter(MF). The other curves represent the same when a MMF is used. The different colors show results for different segmentation of the data. The results show that for low SNRs, the general MF has a slightly better performance. More notably, the results of MMF with 4 segments of the data vector, shows the worst performance. The reason for the latter is that, by using MMF, we assumed that each data segment is quasi-stationary. However, because of the nature of the noise(variance vector has 8 segments), this condition is violated when we use 4 segments. Below SNR 6, the MF perform slightly better because the standard deviation of the noise varies only by a small range($\pm 10\%$), when the signal is present. For this reason, all the curves are close to each other.

part of whole noise. So when we chop data and templates into segments, the output SNR of matched filter enhance compared to general matched filter. And for Fig. 17, since the signal lays in the fluctuating part of the noise, the output SNR of modified matched filter is still much better than general matched filter but not as good as

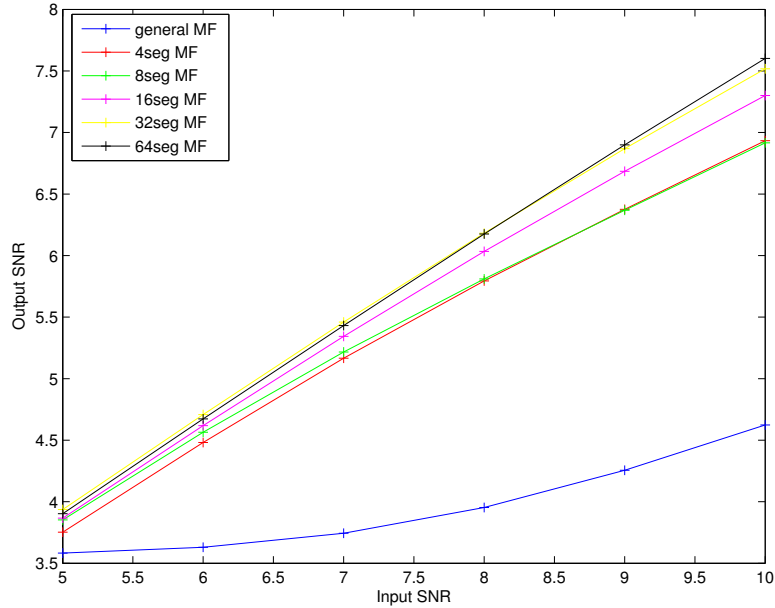


Figure 17: This figure represents the results of detection by the modified matched filter(MMF) with the variance vector divided into 4 segments, when the noise is non-stationary. The the horizontal axis shows the SNR of injected signal and the the vertical axis shows the MF/MMF output SNR. This noise model in this study is shown in Fig. 10 and the chirp signal is injected from 10th second, where the noise varies more than other parts in Fig. 14 bottom panel. The blue curve represents the output of the search using a standard MF. The other curves represent the same when a MMF is used. The different colors show results for different segmentation of the data. Compared with Fig. 15, we can see that here the MMF also has a significantly better performance than a regular MF but the detections are lower than in Fig. 15 since the noise varies more where signal represents.

Fig. 16.

So from the above analysis, we can see that when the signal is located in noise close to stationary, general matched filter can work very well. But if the whole noise is fluctuating, then the detection statistic of general matched filtering is not as good as chopping the data into segments. When the signal is in the stationary part of noise, we drop the non-stationary part of noise, which makes the detection statistic

better.

One important thing we must mention is that when we use the modification of matched filter, where we cut data and signal into different segments, we do re-normalization to the output SNR of matched filter. First, we got the re-normalization factors based on the outputs SNR of white noise, which should be scaled to the inputs SNR. With the re-normalization factors, we divided the outputs SNR of the two non-stationary data sets by it, so they are also scaled to input SNRs. The reason why we do this is that when we use general matched filter, the output is the inner product of data x and $template$. But when we cut the data into segments, we are missing the cross terms, such as inner product of x_1 and $template_2$, and we only use the terms as inner product of x_1 and $template_1$ and so on.

For example, if we cut the data and template into two segments, as shown in Eq. 14

$$\langle x, s \rangle = \langle x_1, s_1 \rangle + \langle x_1, s_2 \rangle + \langle x_2, s_1 \rangle + \langle x_2, s_2 \rangle \quad (14)$$

If we only take $\langle x_1, s_1 \rangle$ and $\langle x_2, s_2 \rangle$ into account, we are missing $\langle x_1, s_2 \rangle$ and $\langle x_2, s_1 \rangle$ terms and the output SNR will not be general output SNR of matched filtering. Thus, we have to renormalize the output and the renormalization constant is defined as the output of white noise divided by the input SNR .

To have an idea about how this method works on LIGO noise, we built a noise set with real LIGO data from 'DARM' and combined with some gaussian modulated sinusoidal pulses. The noise and normalized chirp signal is plotted in Fig. 18

Compared with the above three data sets, we expect the output of matched

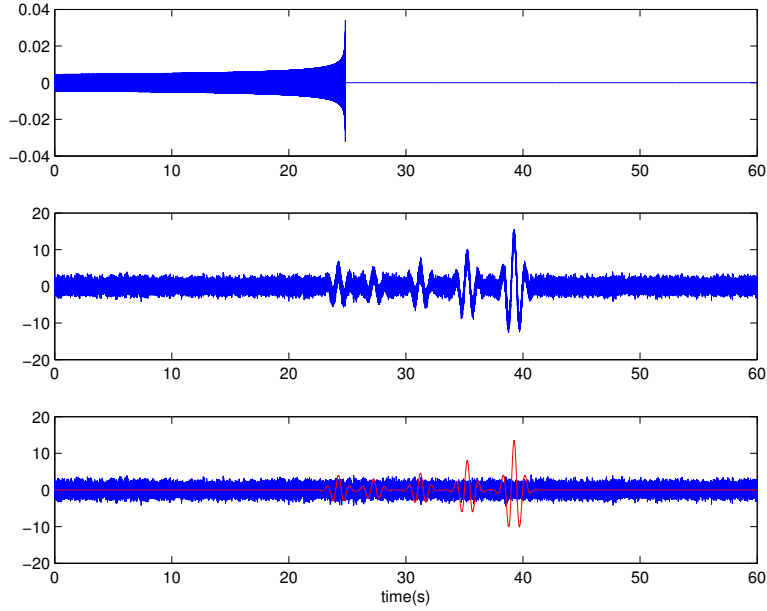


Figure 18: This figure represents injection of a chirp signal with SNR 1 in real LIGO data from the sixth science run(S6). The the horizontal axis is time in seconds and the vertical axis represents the amplitude in arbitrary units. The top panel show the chirp signal that lasts in 24.8381 seconds, the middle and bottom panel show the S6 noise that has been made more non-stationary by a series of gaussian-modulated sinusoidal pulse that mimic glitches seen in real LIGO data.

filter will be like in Fig. 15, where signal is presented when the noise is locally stationary. Our result is shown in Fig. 19(See Appendix B.).

As we expected, the output SNR of matched filter when chopping data and template into segments is better than general matched filter. Here, we did another re-normalization to scale the output SNR according to the output SNR of general matched filter.

In Fig. 15 and Fig. 17, we compared the outputs when arrival time of signal is different. We also repeat it here. We moved the pulse to the beginning, so that the signal is almost present at non-stationary part, shown in Fig. 20. And Fig. 21

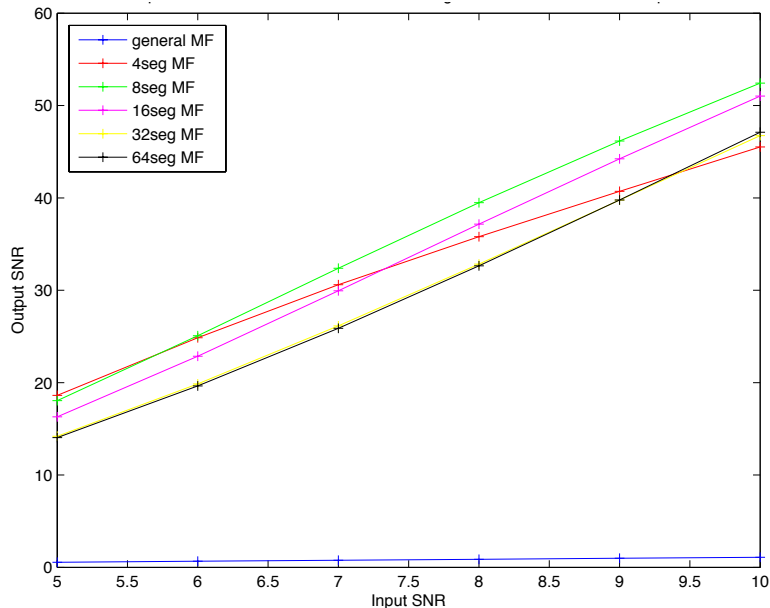


Figure 19: This figure represents the results of detection by the MF/MMF of pulses injected LIGO noise and chirp signal as shown in Fig. 18. The horizontal axis shows the SNR of injected signal and the vertical axis shows the MF/MMF output SNR. The blue curve represents the output of the search using a standard matched filter(MF). The other curves represent the same when a MMF is used. The different colors show results for different segmentation of the data. In this condition, the general definition of SNR doesn't hold, thus the output SNR is different from the general SNR shown in the above figures. But it is clear from the figure that the MMF still has a significantly better performance than a regular MF. The reason for this is that when we use MMF and chop data into smaller segments, the effect of non-stationary is reduced.

is the output.

Here, we see that, if the data is segmented into a smaller numbers of segments, the detection statistic is poor. This is because the nature of the non-stationary present in the data does not support the main assumption that each segment is quasi-stationary. However, as seen in the Fig. 21, if we chop the data into a larger number of segments(like 32 and 64 segments in our simulation), the above assumption is satisfied. Thus the detection statistic is also significantly improved.

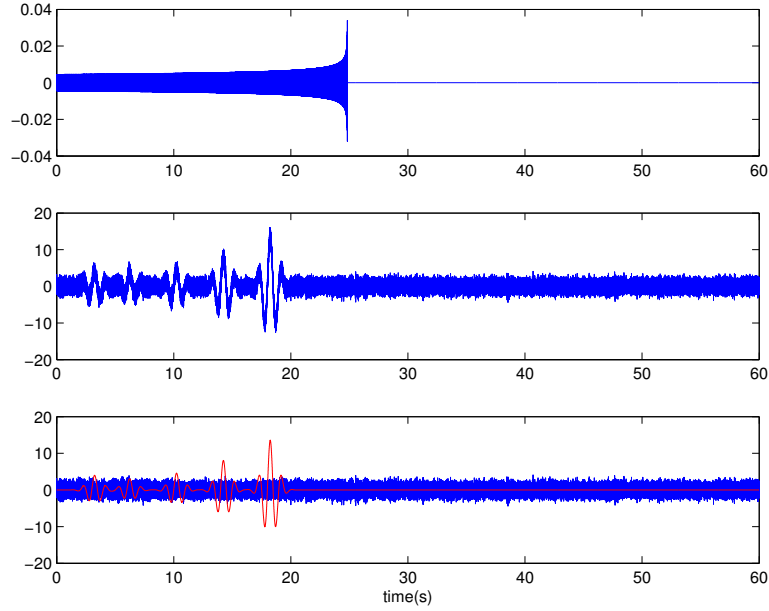


Figure 20: This figure represents injection of a chirp signal with SNR 1 in real LIGO data from the sixth science run(S6). The the horizontal axis is time in seconds and the vertical axis represents the amplitude in arbitrary units. The top panel show the chirp signal that lasts in 24.8381 seconds, the middle and bottom panel show the S6 noise that has been made more non-stationary by a series of gaussian-modulated sinusoidal pulse that mimic glitches seen in real LIGO data. Compared with Fig. 18, the signal lies in the non-stationary part of noise.

From the above results, we can see that if chop data and template into segments, the output of matched filter is better than general matched filter. But, if the signal is present at stationary part of noise, the result will be better because in this way, the non-stationary is taken into account for the segment it relies and will have less affect on the output.

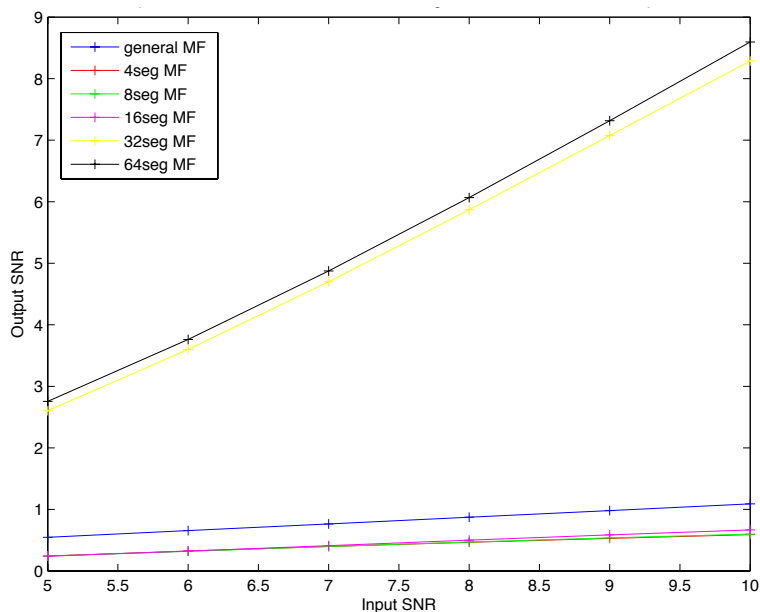


Figure 21: This figure represents the results of detection by the MF/MMF of pulses injected LIGO noise and chirp signal as shown in Fig. 20. The horizontal axis shows the SNR of injected signal and the vertical axis shows the MF/MMF output SNR. The blue curve represents the output of the search using a standard matched filter(MF). The other curves represent the same when a MMF is used. The different colors show results for different segmentation of the data. The difference of this data model in Fig. 20 and Fig. 18 is that here the signal lies in the non-stationary port of noise, but this difference causes a big decrease in detection. Here if the data is chopped into a small numbers of segments, the detection statistic is poor because the nature of the non-stationary present in the data does not support the main assumption that each segment is quasi-stationary. However, if chop the data into a larger number of segments, the above assumption is satisfied. Thus the detection statistic is also significantly improved.

CHAPTER 5

CONCLUSION

In this work, we studied the detection of chirp signals generated by BNS systems using matched filtering method. Matched filtering is a method widely used and sufficient for detection when the detector noise is gaussian and stationary. But if noise is non-stationary, its efficiency decreases. Since GWs are very weak compared with noise, a more robust detection method is needed, even if the noise is non-stationary. Thus, we worked out a modified matched filter to include the time-varying nature of the detector noise.

Before we go to real LIGO data, we first constructed a set of simulated data based on LIGO detector outputs. Firstly, since LIGO noise is non-stationary, we used sinusoidal wave function to simulate different non-stationary noise samples. To compare the efficiency of detection, we also used white gaussian stationary noise. After this, we simulated our chirp signal waveform template based on a binary neutron star system with equal mass $1.4 M_{\odot}$. Then we built our data by injecting the chirp signal into our non-stationary noise sets and also white gaussian noise. In order to see how general matched filtering responds to both non-stationary noise and stationary gaussian noise, we studied the detection statistics, which is the output SNR of matched filter for all data sets. It was found that the efficiency of general matched filtering was weakened when noise became non-stationary, as expected.

The most important part of this research is to study the effects of non-

stationarity noise and how to make the detection more efficient in the presence of non-stationary noise. Keeping in mind that the LIGO noise spectrum changes with time, the calculation of the power spectrum based on the full data segment under investigation is not a true estimate. Since a power spectral estimate plays a direct role in calculation of the matched filter detection efficiency, it is of utmost importance that the changing spectral density is taken into account. We achieve this by constructing a modified matched filter where we chop the data into small quasi-stationary segments and estimate the spectral density. By doing this, we included the non-stationarity of the noise for matched filtering analysis. We then compared the detection of general and modified matched filtering as shown in Fig. 19. As we can see, the modified matched filtering has a significantly better performance.

Our work is original research to study how to modify matched filtering to work more robustly with non-stationary noise. Our immediate goal is to implement this new algorithm on LIGO science data to investigate if the performance shows significant improvement. This will be particularly important in case of Advanced LIGO (aLIGO) where the NS-NS binary signals are expected to stay in the LIGO band for several minutes and thus, we can not afford to miss detecting it, even if the noise becomes non-stationary.

REFERENCES

- [1] Albert Einstein. Die grundlage der allgemeinen relativitätstheorie. *Annalen der Physik*, 354(7):769–822, 1916.
- [2] A. Einstein. Kommentar zu "Hermann Weyl: Gravitation und Elektrizität". *Sitzungsberichte der Königlich Preußischen Akademie der Wissenschaften (Berlin)*, Seite 478., page 478, 1918.
- [3] Albert Einstein. The general theory of relativity. In *The Meaning of Relativity*, pages 54–75. Springer, 1922.
- [4] James B Hartle. *An introduction to Einsteins general relativity*. Pearson Education, Singapore, 2003.
- [5] Warren G Anderson and Jolien DE Creighton. Searches for gravitational waves from binary neutron stars: A review. *Short-Period Binary Stars: Observations, Analyses, and Results*, pages 23–52, 2008.
- [6] Bernard Schutz. *A first course in general relativity*. 2009.
- [7] Kip S Thorne. *Three hundred years of gravitation, ed by Hawking, Stephen W and Israel, Werner*. Cambridge University Press, 1989.
- [8] Éanna É Flanagan and Scott A Hughes. The basics of gravitational wave theory. *New Journal of Physics*, 7(1):204, 2005.
- [9] Russell A Hulse and Joseph H Taylor. Discovery of a pulsar in a binary system. *The Astrophysical Journal*, 195:L51–L53, 1975.
- [10] Joseph H Taylor and Joel M Weisberg. A new test of general relativity-

- gravitational radiation and the binary pulsar psr 1913+ 16. *The Astrophysical Journal*, 253:908–920, 1982.
- [11] BICEP2 Collaboration, P. A. R. Ade, R. W. Aikin, D. Barkats, S. J. Benton, C. A. Bischoff, J. J. Bock, J. A. Brevik, I. Buder, E. Bullock, C. D. Dowell, L. Duband, J. P. Filippini, S. Fliescher, S. R. Golwala, M. Halpern, M. Hasselfield, S. R. Hildebrandt, G. C. Hilton, V. V. Hristov, K. D. Irwin, K. S. Karkare, J. P. Kaufman, B. G. Keating, S. A. Kernasovskiy, J. M. Kovac, C. L. Kuo, E. M. Leitch, M. Lueker, P. Mason, C. B. Netterfield, H. T. Nguyen, R. O’Brien, R. W. Ogburn, IV, A. Orlando, C. Pryke, C. D. Reintsema, S. Richter, R. Schwarz, C. D. Sheehy, Z. K. Staniszewski, R. V. Sudiwala, G. P. Teply, J. E. Tolan, A. D. Turner, A. G. Vieregg, C. L. Wong, and K. W. Yoon. BICEP2 I: Detection Of B-mode Polarization at Degree Angular Scales. *ArXiv e-prints*, March 2014.
- [12] J. Weber. Detection and generation of gravitational waves. *Physical Review*, 117:306–313, Jan 1960.
- [13] BP Abbott, R Abbott, R Adhikari, P Ajith, B Allen, G Allen, RS Amin, SB Anderson, WG Anderson, MA Arain, et al. Ligo: the laser interferometer gravitational-wave observatory. *Reports on Progress in Physics*, 72(7):076901, 2009.
- [14] Alex Abramovici, William E Althouse, Ronald WP Drever, Yekta Gürsel, Seiji Kawamura, Frederick J Raab, David Shoemaker, Lisa Sievers, Robert E Spero, Kip S Thorne, et al. Ligo: The laser interferometer gravitational-wave obser-

- vatory. *Science*, 256(5055):325–333, 1992.
- [15] Barry C Barish and Rainer Weiss. Ligo and the detection of gravitational waves. *Physics Today*, 52:44–50, 1999.
- [16] B Caron, A Dominjon, C Drezen, R Flaminio, X Grave, F Marion, L Massonnet, C Mehmel, R Morand, B Mours, et al. The virgo interferometer. *Classical and Quantum Gravity*, 14(6):1461, 1997.
- [17] Hartmut Grote, LIGO Scientific Collaboration, et al. The geo 600 status. *Classical and Quantum Gravity*, 27(8):084003, 2010.
- [18] Benno Willke, P Aufmuth, C Aulbert, S Babak, R Balasubramanian, BW Barr, S Berukoff, S Bose, G Cagnoli, MM Casey, et al. The geo 600 gravitational wave detector. *Classical and Quantum Gravity*, 19(7):1377, 2002.
- [19] K Kuroda, LCGT collaboration, et al. Status of lqgt. *Classical and Quantum Gravity*, 27(8):084004, 2010.
- [20] Curt Cutler and Kip S Thorne. An overview of gravitational-wave sources. In *Proceedings of the GR16 Conference on General Relativity and Gravitation*, ed. N. Bishop and SD Maharaj (World Scientific, 2002), pages 72–111, 2002.
- [21] Bernard F Schutz. Gravitational-wave sources. *Classical and Quantum Gravity*, 13(11A):A219, 1996.
- [22] Kent Blackburn. The ligo data analysis system: Ldas-a users’ perspective. *LIGO-G990011-00-E*, 1999.
- [23] Stuart Anderson, Keith Riles, Albert Lazzarini, Tom Nash, Alan Weinstein, and Alan Wiseman. Lsc data analysis white paper, draft v. *LIGO Document*

T990104-x0, 2001.

- [24] Nelson Christensen, LIGO Scientific Collaboration, and Virgo Collaboration. Ligo s6 detector characterization studies. *Classical and Quantum Gravity*, 27(19):194010, 2010.
- [25] Gabriela González. Suspensions thermal noise in the ligo gravitational wave detector. *Classical and Quantum Gravity*, 17(21):4409, 2000.
- [26] Gregory M Harry, Andri M Gretarsson, Peter R Saulson, Scott E Kittelberger, Steven D Penn, William J Startin, Sheila Rowan, Martin M Fejer, DRM Crooks, Gianpietro Cagnoli, et al. Thermal noise in interferometric gravitational wave detectors due to dielectric optical coatings. *Classical and Quantum Gravity*, 19(5):897, 2002.
- [27] J Abadie, BP Abbott, R Abbott, TD Abbott, M Abernathy, T Accadia, F Acernese, C Adams, R Adhikari, C Affeldt, et al. Search for gravitational waves from low mass compact binary coalescence in ligo’s sixth science run and virgo’s science runs 2 and 3. *Physical Review D*, 85(8):082002, 2012.
- [28] S.M. Kay. *Fundamentals of Statistical Signal Processing: Detection theory*. Prentice Hall Signal Processing Series. Prentice-Hall PTR, 1998.
- [29] BS Sathyaprakash and SV Dhurandhar. Choice of filters for the detection of gravitational waves from coalescing binaries. *Physical Review D*, 44(12):3819, 1991.
- [30] Stephen Privitera, Satyanarayan RP Mohapatra, Parameswaran Ajith, Kipp Cannon, Nickolas Fotopoulos, Melissa A Frei, Chad Hanna, Alan J Weinstein,

- and John T Whelan. Improving the sensitivity of a search for coalescing binary black holes with nonprecessing spins in gravitational wave data. *Physical Review D*, 89(2):024003, 2014.
- [31] Yan Wang and Soumya D Mohanty. Particle swarm optimization and gravitational wave data analysis: Performance on a binary inspiral testbed. *Physical Review D*, 81(6):063002, 2010.
- [32] SD Mohanty and SV Dhurandhar. Hierarchical search strategy for the detection of gravitational waves from coalescing binaries. *Physical Review D*, 54(12):7108, 1996.
- [33] James A Sills and Edward W Kamen. Time-varying matched filters. *Circuits, Systems and Signal Processing*, 15(5):609–630, 1996.

APPENDIX A CHIRP SIGNAL

```

% chirp signal,Physical Review Volume 54, Number 12
clear all
clc
m1=1.4; % mass of one of the binaries,base Msun
m2=1.4;
fa=40; % low frequency
fc=1000; % stop frequency
fs=2048; % sampling frequency
ta=0; % arrival time of the signal
r=38; % distance of binaries
PHI=0; % initial phase

M=((m1*m2)/(m1+m2))^3*(m1+m2)^2^(1/5); % mass funtion
chirptime=34.54*(M)^(-5/3)*(fa/40)^(-8/3); % chirp time
A=1.92*10^(-23)*(chirptime/25)^(-1)*(r/100)^(-1)*(fa/40)^(-2);
% part of amplitude r base 100Mpc fa base 40Hz
tc=(1-(fa/fc)^(8/3))*chirptime; % time when frequency is 1000Hz
tchirp=0:1/fs:tc; % time vector of the signal
a=(1-tchirp/chirptime).^(-1/4); % part of amplitude
phi=((8*chirptime*fa)/5-(8*chirptime*fa*(1 - tchirp/chirptime).^(5/8))/5);
% phase changing with time
h0=a.*cos(phi); % initial phase PHI=0
h2=a.*cos(phi+pi/2); % initial phase PHI=PI/2
h=A*h0*cos(PHI)+A*h2*sin(PHI); % wave form
figure
plot(tchirp,h)
title('Chirp Signal')
xlabel('time(s)')
ylabel('strain of chirp signal')

```

APPENDIX B

OUTPUT OF MATCHED FILTER FOR LIGO AND GAUSSIANSINE DATA

```

% chirp signal,Physical Review Volume 54, Number 12
% Code for 8,16,32,64 Segments for three different sets of noise with SNR 5
% to 10
% rdata: normalized clean data of 1H.DARM
% gausinpl: gaussian pulse

clear all
clc

%%

T=60; % data length 60s
fs=2048; % sampling frequency
Ns=T*fs;
deltaT=1/fs;
deltaF=1/T;
Tvector=(0:Ns-1)/fs;

%% Parameters of Binaries

m1=1.4; % mass of one of the binaries,base Msun
m2=1.4;
r=38; % distance of binaries, based on 100 Mpc

%% Initials of templates

fa=40; % low cutoff frequency
fc=1000; % high cutoff frequency
ta=0; % arrival time of the signal
PHI0=0;
phi0=0;
phi2=pi/2;
tah=0; % time of arrival for template

%% chirp signal

M=((m1*m2)/(m1+m2))^3*(m1+m2)^2^(1/5); % mass funtion
chirptime=34.54*(M)^(-5/3)*(fa/40)^(-8/3); % chirp time
tc=(1-(fa/fc)^(8/3))*chirptime; % time at 1000Hz
A=1.92*10^(-23)*(chirptime/25)^(-1)*(r/100)^(-1)*(fa/40)^(-2);
% part of amplitude r base 100Mpc fa base 40Hz,related to detection
% statistic
tchirp=0:deltaT:tc; % time vector of the chirp
a=(1-tchirp/chirptime).^(-1/4); % part of amplitude
phi=2*pi*(8/5)*chirptime*fa*(1-(1-tchirp/chirptime).^(5/8)); % phase
h01=A*a.*cos(phi); % PHI=0 template

```

```

h0=[h01 zeros(1,Ns-length(h01))]; % original phase is 0 template

h901=A*a.*cos(phi+pi/2); % original phase=PI/2
h90=[h901 zeros(1,Ns-length(h901))];
chirpS=[h01 zeros(1,Ns-length(h01))];
%% FFT frequency

% Frequency of FFT for whole data
Nfreq=(0:(Ns/2))/T;
% interpolate frequency for positive frequencies
NfreqInverse=fliplr(Nfreq); % inverse of interpolate frequency
NfreqV=[Nfreq NfreqInverse(2:Ns/2+1)]; % interpolate frequency

% Frequency Vector of FFT of Segment

Len_seg1=Ns/4;
Nfreqs1=(0:Len_seg1/2)*fs/Len_seg1;
NfreqsInverse1=fliplr(Nfreqs1); % inverse of interpolate frequency
NfreqsV1=[Nfreqs1 NfreqsInverse1(2:Len_seg1/2+1)]; % interpolate frequency

Len_seg2=Ns/8;
Nfreqs2=(0:Len_seg2/2)*fs/Len_seg2;
NfreqsInverse2=fliplr(Nfreqs2); % inverse of interpolate frequency
NfreqsV2=[Nfreqs2 NfreqsInverse2(2:Len_seg2/2+1)]; % interpolate frequency

Len_seg3=Ns/16;
Nfreqs3=(0:Len_seg3/2)*fs/Len_seg3;
NfreqsInverse3=fliplr(Nfreqs3); % inverse of interpolate frequency
NfreqsV3=[Nfreqs3 NfreqsInverse3(2:Len_seg3/2+1)]; % interpolate frequency

Len_seg4=Ns/32;
Nfreqs4=(0:Len_seg4/2)*fs/Len_seg4;
NfreqsInverse4=fliplr(Nfreqs4); % inverse of interpolate frequency
NfreqsV4=[Nfreqs4 NfreqsInverse2(2:Len_seg4/2+1)]; % interpolate frequency

Len_seg5=Ns/64;
Nfreqs5=(0:Len_seg5/2)*fs/Len_seg5;
NfreqsInverse5=fliplr(Nfreqs5);
% inverse of interpolate frequency
NfreqsV5=[Nfreqs5 NfreqsInverse5(2:Len_seg5/2+1)];
% interpolate frequency
%% LIGO data
ligo.noise=load('rdatam.txt');
ligo.noise=(ligo.noise-mean(ligo.noise))/std(ligo.noise);
%% Gaussian Modulated Sinusoidal Pulse
tg = gausspuls('cutoff',50e1,0.6,[],-1000); % Initial gaussian pulse
gausin.vector = -tg : 1e-6 : tg; % time vector
[gausinpl,ps.injection]=GaussianSineUniform(gausin.vector,Ns,fs);
gausinpl=[gausinpl(1,10*fs+1:Ns) zeros(1,10*fs)];
%% Combined noise with Ligo noise and gaussian pulse
nonstat_noise_1=ligo.noise+gausinpl;
%% Matched Filtering

```

```

for i=1:10000

    wn=randn(1,Ns);
    wn=(wn-mean(wn))/std(wn);

    [P_wn,F_wn]=pwelch(wn,fs/4,[],fs/4,fs); % get PSD of noise using pwelch
    P_wn=P_wn*fs/2; % fs/2 is scalar factor
    Npsd=interp1(F_wn,P_wn,NfreqV); % noise psd after interpolation
    Npsd=Npsd(1,1:end-1);

    % Normlize Constant and Normlization of Signal
    NormConst=sqrt(Ns)/sqrt(sum(fft(h0).*conj(fft(h0))./Npsd));
    h0N=h0*NormConst;
    h90N=h90*NormConst;
    S_chirp=chirpS*NormConst;

    fft_S=fft(S_chirp); % chirp signal template injected into noise

    %nonstat_noise_1=sigmaV_1.*wn; % nonstatnoise set
    [P_n1,F_n1]=pwelch(nonstat_noise_1,fs/4,[],fs/4,fs);
    % get PSD of noise using pwelch
    P_n1=P_n1*fs/2; % fs/2 is scalar factor
    Npsd_n1=interp1(F_n1,P_n1,NfreqV); % noise psd after interpolation
    Npsd_n1=Npsd_n1(1,1:end-1);

    for SNR=5:10
        x_wn=wn+S_chirp*SNR;
        xn1=nonstat_noise_1+S_chirp*SNR; % data set
        InPr0n_1=ifft(fft(xn1).*conj(fft(h0N))./Npsd_n1);
        InPr90n_1=ifft(fft(xn1).*conj(fft(h90N))./Npsd_n1);
        lamdaAG_1=sqrt((abs(InPr0n_1).^2+(abs(InPr90n_1).^2)));
        detanG_1(SNR-4,i)=max(lamdaAG_1);
        % output of Matched Filtering
        l=1;
        % Output of Matched Filtering Using Segments
        for lv=0:Len_seg1:Ns-Len_seg1

            fft_h0N_4=fft(h0N(1,lv+1:lv+Len_seg1));
            fft_h90N_4=fft(h90N(1,lv+1:lv+Len_seg1));

            [P_wn_4,F_wn_4]=pwelch(wn(1,lv+1:lv+Len_seg1),fs/4,[],fs/4,fs);
            P_wn_4=P_wn_4*fs/2;
            Npsd_4=interp1(F_wn_4,P_wn_4,NfreqsV1);
            Npsd_4=Npsd_4(1,1:end-1);

            [P_n1_4,F_n1_4]=pwelch(nonstat_noise_1(1,lv+1:lv+Len_seg1),...
                fs/4,[],fs/4,fs);
            P_n1_4=P_n1_4*fs/2;
            Npsd_n1_4=interp1(F_n1_4,P_n1_4,NfreqsV1);
            Npsd_n1_4=Npsd_n1_4(1,1:end-1);

            fft_wn=fft(x_wn(1,lv+1:lv+Len_seg1));

```

```

InPr0n_4=ifft(fft_wn.*conj(fft_h0N_4)./Npsd_4);
InPr90n_4=ifft(fft_wn.*conj(fft_h90N_4)./Npsd_4);
lamdaAM_wn=sqrt((abs(InPr0n_4)).^2+(abs(InPr90n_4)).^2);
detansM_wn(1)=max(lamdaAM_wn);

fft_x1=fft(xn1(1,lv+1:lv+Len_seg1));
InPr0n_x1=ifft(fft_x1.*conj(fft_h0N_4)./Npsd_n1_4);
InPr90n_x1=ifft(fft_x1.*conj(fft_h90N_4)./Npsd_n1_4);
lamdaAM_x1=sqrt((abs(InPr0n_x1)).^2+(abs(InPr90n_x1)).^2);
detansM_x1(1)=max(lamdaAM_x1);
l=l+1;

end
D_wn_4(SNR-4,i)=sum(detansM_wn);
detanM_x1_4(SNR-4,i)=sum(detansM_x1);
clear fft_wn InPr0n_4 InPr90n_4 lamdaAM_wn detansM_wn...
      fft_x1 InPr0n_x1 InPr90n_x1 lamdaAM_x1 detansM_x1

l=1;
for lv=0:Len_seg2:Ns-Len_seg2

    fft_h0N_8=fft(h0N(1,lv+1:lv+Len_seg2));
    fft_h90N_8=fft(h90N(1,lv+1:lv+Len_seg2));

    [P_wn_8,F_wn_8]=pwelch(wn(1,lv+1:lv+Len_seg2),fs/4,[],fs/4,fs);
    P_wn_8=P_wn_8*fs/2;
    Npsd_8=interp1(F_wn_8,P_wn_8,NfreqsV2);
    Npsd_8=Npsd_8(1,1:end-1);

    [P_n1_8,F_n1_8]=pwelch(nonstat_noise_1(1,lv+1:lv+Len_seg2),...
        fs/4,[],fs/4,fs);
    P_n1_8=P_n1_8*fs/2;
    Npsd_n1_8=interp1(F_n1_8,P_n1_8,NfreqsV2);
    Npsd_n1_8=Npsd_n1_8(1,1:end-1);

    fft_wn=fft(x_wn(1,lv+1:lv+Len_seg2));
    InPr0n_8=ifft(fft_wn.*conj(fft_h0N_8)./Npsd_8);
    InPr90n_8=ifft(fft_wn.*conj(fft_h90N_8)./Npsd_8);
    lamdaAM_wn=sqrt((abs(InPr0n_8)).^2+(abs(InPr90n_8)).^2);

    detansM_wn(1)=max(lamdaAM_wn);

    fft_x1=fft(xn1(1,lv+1:lv+Len_seg2));
    InPr0n_x1=ifft(fft_x1.*conj(fft_h0N_8)./Npsd_n1_8);
    InPr90n_x1=ifft(fft_x1.*conj(fft_h90N_8)./Npsd_n1_8);
    lamdaAM_x1=sqrt((abs(InPr0n_x1)).^2+(abs(InPr90n_x1)).^2);
    detansM_x1(1)=max(lamdaAM_x1);

    l=l+1;

end
D_wn_8(SNR-4,i)=sum(detansM_wn);
detanM_x1_8(SNR-4,i)=sum(detansM_x1);
clear fft_wn InPr0n_8 InPr90n_8 lamdaAM_wn detansM_wn...

```

```

fft_x1 InPr0n_x1 InPr90n_x1 lamdaAM_x1 detansM_x1
l=1;
for lv=0:Len_seg3:Ns-Len_seg3

fft_h0N_16=fft(h0N(1,lv+1:lv+Len_seg3));
fft_h90N_16=fft(h90N(1,lv+1:lv+Len_seg3));

[P_wn_16,F_wn_16]=pwelch(wn(1,lv+1:lv+Len_seg3),fs/4,[],...
    fs/4,fs);
P_wn_16=P_wn_16*fs/2;
Npsd_16=interp1(F_wn_16,P_wn_16,Nfreqs3);
Npsd_16=[Npsd_16 Npsd_16(1,end-1:-1:2)];

[P_n1_16,F_n1_16]=pwelch(nonstat_noise_1(1,lv+1:lv+Len_seg3),...
    fs/4,[],fs/4,fs);
P_n1_16=P_n1_16*fs/2;
Npsd_n1_16=interp1(F_n1_16,P_n1_16,Nfreqs3);
Npsd_n1_16=[Npsd_n1_16 Npsd_n1_16(1,end-1:-1:2)];

fft_wn=fft(x_wn(1,lv+1:lv+Len_seg3));
InPr0n_16=ifft(fft_wn.*conj(fft_h0N_16)./Npsd_16);
InPr90n_16=ifft(fft_wn.*conj(fft_h90N_16)./Npsd_16);
lamdaAM_wn=sqrt((abs(InPr0n_16)).^2+(abs(InPr90n_16)).^2);

detansM_wn(1)=max(lamdaAM_wn);

fft_x1=fft(xn1(1,lv+1:lv+Len_seg3));
InPr0n_x1=ifft(fft_x1.*conj(fft_h0N_16)./Npsd_n1_16);
InPr90n_x1=ifft(fft_x1.*conj(fft_h90N_16)./Npsd_n1_16);
lamdaAM_x1=sqrt((abs(InPr0n_x1)).^2+(abs(InPr90n_x1)).^2);
detansM_x1(1)=max(lamdaAM_x1);

l=l+1;
end
D_wn_16(SNR-4,i)=sum(detansM_wn);
detanM_x1_16(SNR-4,i)=sum(detansM_x1);

clear fft_wn InPr0n_16 InPr90n_16 lamdaAM_wn detansM_wn...
fft_x1 InPr0n_x1 InPr90n_x1 lamdaAM_x1 detansM_x1
l=1;
for lv=0:Len_seg4:Ns-Len_seg4

fft_h0N_32=fft(h0N(1,lv+1:lv+Len_seg4));
fft_h90N_32=fft(h90N(1,lv+1:lv+Len_seg4));

[P_wn_32,F_wn_32]=pwelch(wn(1,lv+1:lv+Len_seg4),fs/4,[],fs/4,fs);
P_wn_32=P_wn_32*fs/2;
Npsd_32=interp1(F_wn_32,P_wn_32,Nfreqs4);
Npsd_32=[Npsd_32 Npsd_32(1,end-1:-1:2)];

[P_n1_32,F_n1_32]=pwelch(nonstat_noise_1(1,lv+1:lv+Len_seg4),...
    fs/4,[],fs/4,fs);
P_n1_32=P_n1_32*fs/2;

```

```

Npsd_n1_32=interp1(F_n1_32,P_n1_32,Nfreqs4);
Npsd_n1_32=[Npsd_n1_32 Npsd_n1_32(1,end-1:-1:2)];

fft_wn=fft(x_wn(1,lv+1:lv+Len_seg4));
InPr0n_32=ifft(fft_wn.*conj(fft_h0N_32)./Npsd_32);
InPr90n_32=ifft(fft_wn.*conj(fft_h90N_32)./Npsd_32);
lamdaAM_wn=sqrt((abs(InPr0n_32)).^2+(abs(InPr90n_32)).^2);

detansM_wn(1)=max(lamdaAM_wn);

fft_x1=fft(xn1(1,lv+1:lv+Len_seg4));
InPr0n_x1=ifft(fft_x1.*conj(fft_h0N_32)./Npsd_n1_32);
InPr90n_x1=ifft(fft_x1.*conj(fft_h90N_32)./Npsd_n1_32);
lamdaAM_x1=sqrt((abs(InPr0n_x1)).^2+(abs(InPr90n_x1)).^2);
detansM_x1(1)=max(lamdaAM_x1);

l=l+1;
end
D_wn_32(SNR-4,i)=sum(detansM_wn);
detanM_x1_32(SNR-4,i)=sum(detansM_x1);
clear fft_wn InPr0n_32 InPr90n_32 lamdaAM_wn detansM_wn...
      fft_x1 InPr0n_x1 InPr90n_x1 lamdaAM_x1 detansM_x1
l=1;
for lv=0:Len_seg5:Ns-Len_seg5

fft_h0N_64=fft(h0N(1,lv+1:lv+Len_seg5));
fft_h90N_64=fft(h90N(1,lv+1:lv+Len_seg5));

[P_wn_64,F_wn_64]=pwelch(wn(1,lv+1:lv+Len_seg5),fs/4,[],fs/4,fs);
P_wn_64=P_wn_64*fs/2;
Npsd_64=interp1(F_wn_64,P_wn_64,Nfreqs5);
Npsd_64=[Npsd_64 Npsd_64(1,end-1:-1:2)];

[P_n1_64,F_n1_64]=pwelch(nonstat_noise_1(1,lv+1:lv+Len_seg5),...
      fs/4,[],fs/4,fs);
P_n1_64=P_n1_64*fs/2;
Npsd_n1_64=interp1(F_n1_64,P_n1_64,Nfreqs5);
Npsd_n1_64=[Npsd_n1_64 Npsd_n1_64(1,end-1:-1:2)];

fft_wn=fft(x_wn(1,lv+1:lv+Len_seg5));
InPr0n_64=ifft(fft_wn.*conj(fft_h0N_64)./Npsd_64);
InPr90n_64=ifft(fft_wn.*conj(fft_h90N_64)./Npsd_64);
lamdaAM_wn=sqrt((abs(InPr0n_64)).^2+(abs(InPr90n_64)).^2);

detansM_wn(1)=max(lamdaAM_wn);

fft_x1=fft(xn1(1,lv+1:lv+Len_seg5));
InPr0n_x1=ifft(fft_x1.*conj(fft_h0N_64)./Npsd_n1_64);
InPr90n_x1=ifft(fft_x1.*conj(fft_h90N_64)./Npsd_n1_64);
lamdaAM_x1=sqrt((abs(InPr0n_x1)).^2+(abs(InPr90n_x1)).^2);
detansM_x1(1)=max(lamdaAM_x1);

l=l+1;

```

```

end
D_wn_64 (SNR-4, i)=sum(detansM.wn);
detanM_x1_64 (SNR-4, i)=sum(detansM.x1);
clear fft_wn InPr0n_4 InPr90n_4 lamdaAM.wn detansM.wn...
      fft_x1 InPr0n_x1 InPr90n_x1 lamdaAM_x1 detansM_x1

end

end

mean_detanG_LIGO=[mean(detanG_1(1,:)) mean(detanG_1(2,:))...
      mean(detanG_1(3,:)) mean(detanG_1(4,:))...
      mean(detanG_1(5,:)) mean(detanG_1(6,:))];
mean_wn_LIGO_4=[mean(D_wn_4(1,:)) mean(D_wn_4(2,:)) mean(D_wn_4(3,:))...
      mean(D_wn_4(4,:)) mean(D_wn_4(5,:)) mean(D_wn_4(6,:))];
mean_wn_LIGO_8=[mean(D_wn_8(1,:)) mean(D_wn_8(2,:)) mean(D_wn_8(3,:))...
      mean(D_wn_8(4,:)) mean(D_wn_8(5,:)) mean(D_wn_8(6,:))];
mean_wn_LIGO_16=[mean(D_wn_16(1,:)) mean(D_wn_16(2,:)) mean(D_wn_16(3,:))...
      mean(D_wn_16(4,:)) mean(D_wn_16(5,:)) mean(D_wn_16(6,:))];
mean_wn_LIGO_32=[mean(D_wn_32(1,:)) mean(D_wn_32(2,:)) mean(D_wn_32(3,:))...
      mean(D_wn_32(4,:)) mean(D_wn_32(5,:)) mean(D_wn_32(6,:))];
mean_wn_LIGO_64=[mean(D_wn_64(1,:)) mean(D_wn_64(2,:)) mean(D_wn_64(3,:))...
      mean(D_wn_64(4,:)) mean(D_wn_64(5,:)) mean(D_wn_64(6,:))];
mean_xLIGO_4=[mean(detanM_x1_4(1,:)) mean(detanM_x1_4(2,:))...
      mean(detanM_x1_4(3,:)) mean(detanM_x1_4(4,:)) mean(detanM_x1_4(5,:))...
      mean(detanM_x1_4(6,:))];
mean_xLIGO_8=[mean(detanM_x1_8(1,:)) mean(detanM_x1_8(2,:))...
      mean(detanM_x1_8(3,:)) mean(detanM_x1_8(4,:)) mean(detanM_x1_8(5,:))...
      mean(detanM_x1_8(6,:))];
mean_xLIGO_16=[mean(detanM_x1_16(1,:)) mean(detanM_x1_16(2,:))...
      mean(detanM_x1_16(3,:)) mean(detanM_x1_16(4,:))...
      mean(detanM_x1_16(5,:)) mean(detanM_x1_16(6,:))];
mean_xLIGO_32=[mean(detanM_x1_32(1,:)) mean(detanM_x1_32(2,:))...
      mean(detanM_x1_32(3,:)) mean(detanM_x1_32(4,:))...
      mean(detanM_x1_32(5,:)) mean(detanM_x1_32(6,:))];
mean_xLIGO_64=[mean(detanM_x1_64(1,:)) mean(detanM_x1_64(2,:))...
      mean(detanM_x1_64(3,:)) mean(detanM_x1_64(4,:))...
      mean(detanM_x1_64(5,:)) mean(detanM_x1_64(6,:))];

```